Heliyon 10 (2024) e33656

Contents lists available at ScienceDirect

Heliyon

journal homepage: www.cell.com/heliyon

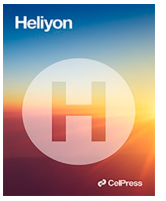

Research article

Design and synthesis of LDH nano composite functionalized with trimesic acid and its environmental application in adsorbing organic dyes indigo carmine and methylene blue

Hoda salamaat, Hossein Ghafuri *, Nastaran Ghanbari

Catalysts and Organic Synthesis Research Laboratory, Department of Chemistry, Iran University of Science and Technology, Tehran, 16846-13114, Iran

ARTICLE INFO

Keywords:
Layered double hydroxide (LDH)
Trimesic acid (TMA)
Indigo carmine (IC)
Methylene blue (MB)

ABSTRACT

This work designed and prepared an organic-inorganic nanocomposite using layered double hydroxide (LDH) inorganic substrate and trimesic acid (TMA) as chelating agent. Subsequently, the synthesized organic-inorganic nanocomposite was assessed using multiple identification methods, including FTIR, EDX, XRD, TGA, and FESEM, and the outcomes demonstrated that the intended structure was successfully prepared. Also, in order to investigate the efficiency of the Mg–Al LDH-TMA nanocomposite as an efficient nano adsorbent, it was used for removal of indigo carmine (IC) and methylene blue (MB) from aqueous solutions. This synthetic nanocomposite showed a high adsorption capacity. The efficiency of the produced nanocomposite in the adsorption of selected dyes was investigated with the help of batch adsorption studies performed in a variety of experimental settings, including dye concentration, adsorbent dose, pH, adsorption temperature and contact time. Furthermore, the produced Mg–Al LDH-TMA nanocomposite exhibits strong stability and can be recycled and reused five times in a row, which is well consistent with the principles of green chemistry.

1. Introduction

Since many of industries have numerous water consumption (as one of the practical requirements for the construction and completion processes), they generate a considerable of sewage, which they discharge into natural bodies of water include rivers, lakes, and oceans. Dyes, despite their wide range of uses, are among the most dangerous and common substances found in the effluent of many different industries, including textile, paper, paint, cosmetics, plastics, food processing, etc. [1]. Even though dyes are essential for the production methods used today, their improper disposal or release into water sources can have detrimental consequences on the environment and public health. It is challenging to the decomposition the dyes because of their strong resistance to biological degradation or photodegradation [2] and they have direct allergic, carcinogenic, and mutagenic impacts on human health as well as their indirect effects through the food chain [3–6]. While some coloured wastewater is recovered and utilized again, the majority ends up going into drains where it contaminates the environment [7]. Therefore, one of the fundamental environmental issues facing the globe today is dyes contaminating water [8–10].

These harmful dyes have been eliminated from water over the past few decades using a variety of approaches, including chemical

* Corresponding author.
E-mail address: ghafuri@iust.ac.ir (H. Ghafuri).

https://doi.org/10.1016/j.heliyon.2024.e33656
Received 1 February 2024; Received in revised form 24 June 2024; Accepted 25 June 2024
Available online 26 June 2024

[11], electrochemical [12], ozonation [13], photocatalytic degradation [14,15], biodegradation [16], and adsorption techniques [17]. However, nearly all of these techniques are inefficient and have a number of drawbacks, including the producing a large amount of sludge, high costs, high energy consumption, the generation of harmful by-products, etc [2]. Adsorption is an excellent approach among them because it is inexpensive, efficient across a broad pH range, adsorbent renewal ability, simple operation, and high yield [18–20]. Adsorption is thus considered as the most effective and popular water treatment method [21,22].

Different and special adsorbents, including layered-double hydroxides, CNTs (Carbon nanotubes) [23,24], graphene oxide [25], agricultural waste [26,27], activated carbons [28], clay [29], zeolite [30], polymers [31,32], Covalent organic frameworks (COFs) are a class of crystalline porous polymers possessing large surface area, nanoporous properties, and superior thermal stability [33,34], Mixed metal sulphides (MMSs) because of their better electrical and redox reactions [35], reactive oxygen species (ROS) are widely recognized to comprise both superoxide ($\cdot O_2^-$) and hydroxyl ($\cdot OH^-$) radicals [36], were investigated to evaluate their ability for water treatment. While, adsorbents derived from layered double hydroxides (LDH) due to their outstanding adsorption abilities, this adsorbent are a class of adaptable materials that have attracted substantial attention in numerous scientific and industrial domains. LDHs are also known as hydrotalcite-like compounds are a class of ionic layered compounds, they made from the juxtaposition of the positively charged main lamellar of mixed metal hydroxides (which includes trivalent and divalent metals cations that are octahedrally surrounded by hydroxide agents), and an interlamellar region containing different anionic groups (charge-compensation groups) and small solvent molecules. LDH's general formula is often expressed as: $[M^{2+}_{1-x}M^{3+}_x(OH)_2][A^{n-}]_{x/n}\cdot mH_2O$, which M^{+2} represents divalent cations (Ni^{2+}, Zn^{2+}, Cu^{2+}, Mg^{2+}), while M^{+3} shows trivalent cations (Ga^{3+}, Al^{3+}, Fe^{3+}), A^{n-} Expressing interlamellar anionic groups (CO_3^{2-}, NO_3^-, SO_4^{2-}, Cl^-), X is a constant number and usually its value is between 0.20 and 0.33, which is obtained from the ratio of M^{+3} + M^{+2}/M^{+3} [37–42].

Due to their distinctive layered structure, LDH-based adsorbents have strong adsorption efficiency for removing anionic or cationic pollutants by ion exchange with M^{2+} ions in LDH due to the large interlayer gap that allows them to exchange anion ions and a positive charge layer. LDH adsorbents have many uses in wastewater treatment, environmental remediation, and the elimination of different contaminants from aqueous solutions. They are especially good at adsorbing anionic pollutants such organic dyes, heavy metal ions, and anionic organic chemicals. LDHs are extremely flexible to different adsorption requirements since their surface characteristics and composition may be customized. The good adsorption capacity, selectivity, and simplicity of regeneration of LDH adsorbents are benefits. They are also regarded as sustainable and environmentally friendly due to their natural abundance and minimal toxicity. The elimination of dangerous compounds from industrial processes and other urgent global concerns like water contamination hold promise for these materials.

Indigo carmine (IC) is one of the anionic organic dyes soluble in water. This dye is used for medical diagnostic purposes in addition to its widespread application in the food industries (such as baked goods, sweets, confectionery, ice creams, sauces, chewing gums, and flavored drinks) [43,44] It is also used as a fabric dyeing agent and in analytical chemistry to detect redox reactions [45]. Even though the European Union and the US have approved IC [43], it is still regarded as a highly hazardous dye that, when exposed to, can have serious negative effects on human health, including carcinogenesis, respiratory issues, neurotoxicity, and eye and skin irritation (Scheme 1b) [46]. Methylene blue (MB) is a cationic blue dye that contains sulfur and belonging to the phenothiazine family. It is used in many commercial processes, including the dyeing of silk, cotton, and wool as well as the production of paper. It can also serve as an indication of oxidation and reduction reaction [47–49]. After inhalation, it can result in symptoms like nausea, diarrhea, breathing

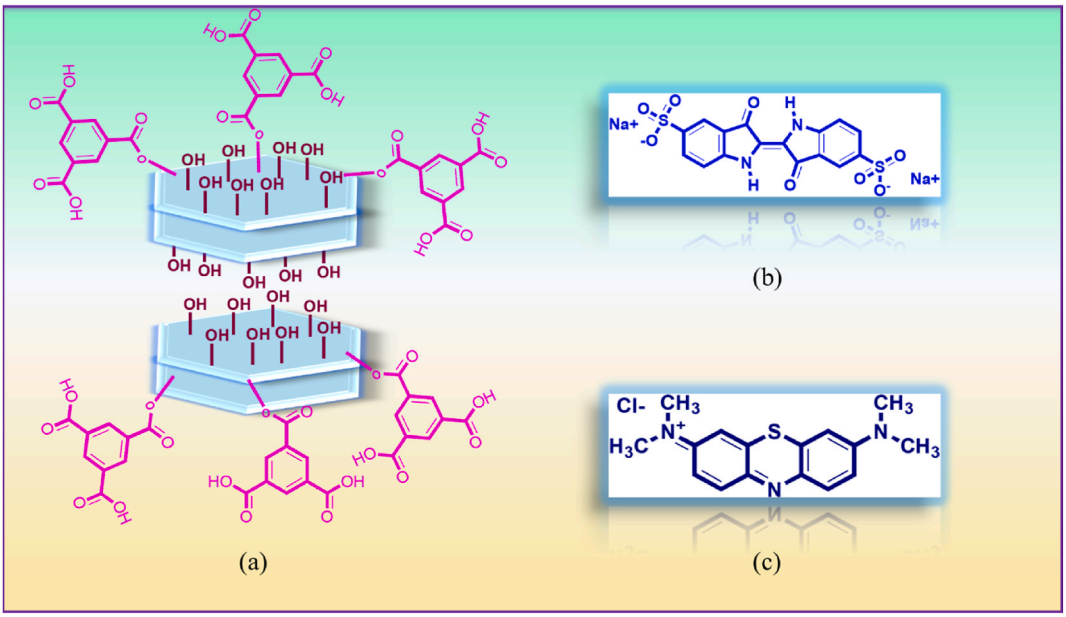

Scheme 1. LDH–TMA nanocomposite (a), Indigo carmine (b) and Methylene blue structure (c).

difficulties, and vomiting in humans. It can also result in eye burning or even permanent eye damage (Scheme 1c) [50].

The development of a modified LDH with TMA as a nanocomposite to remove IC and MB from aqueous solutions is the benefit of this work. Due to the existence of lone pair electrons in oxygenated functional groups available in TMA such as hydroxyl and carboxylic acid groups as chelating groups It causes this synthesized nanocomposite has shown a high adsorption capacity. The efficacy of the generated nanocomposite in adsorbing selected dyes was investigated with the aid of batch sorption studies conducted under a variety of experimental settings, including dye concentration, adsorbent dose, pH, adsorption temperature, and contact time. The adsorption of MB and IC process was studied using data from several adsorption models and nanocomposite isotherms. This study seeks to advance knowledge of how to prepare Mg–Al-LDH-TMA with improved sorption performance and removal efficiency for the MB and IC dyes using a Coprecipiation methodology. This is an efficient, cost-effective, and environmentally friendly strategy for dye removal in real environmental control and remediation (Scheme 1a).

2. Experimental

2.1. Reagents and apparatus

All the chemicals reagents used were analytical grade and were purchased from Merck or Aldrich and it is used without any second treatment. Characterization of the LDH-trimesic acid nanocomposite was performed by FESEM (ZEISS-SIGMA300), EDX (Numerix DXP-X10P), FTIR (Shimadzu 8400 s), and TGA (Bahr Company STA 504). XRD patterns of the LDH-trimesic acid nanocomposite was obtained using TW 1800 diffractometer with Cu_{Ka} radiation ($\lambda = 1.54050$ Å).

2.2. Preparation method of Mg–Al LDH

Mg–Al LDH was prepared using previously reported methods. Mg–Al LDH was synthesized using the co-precipitation method with urea solution assistance. First, 100 mL of 3 M urea solution was prepared, then it was transferred to a round bottom glass flask (200 mL), and 3.75 g $Al(NO_3)_3.9H_2O$ and 5.13 g $Mg(NO_3)_2.6H_2O$ were added to the above solution under stirring conditions and then it was refluxed and stirred for 12 h at 100 ℃. After stirring for 12 h the temperature is reduced by 6 ℃ and reflux the obtained suspension for another 12 h under static conditions. Ultimately, the precipitate particles were centrifuged collected, repeatedly washed in a solution of water and EtOH, and then dried for 24 h at 80 °C (Scheme 2).

2.3. Preparation method of TMA-Cl

A mixture of toluene (20 mL) and trimesic acid (TMA, 2.0 g) were stirred at room temperature for 5 min until the material was completely dissolved. Then thionyl chloride ($SOCl_2$,0.7 mL) was added dropwise to the previous solution in a glass flask, the reflux condenser was attached and the mixture reaction kept at 70 °C under reflux circumstances for 24 h. Then a rotary evaporator was used to remove the solvent from reaction mixtures, and subsequent the obtained precipitate was recovered after washing with dichloromethane solvent for a number of times (Scheme 3).

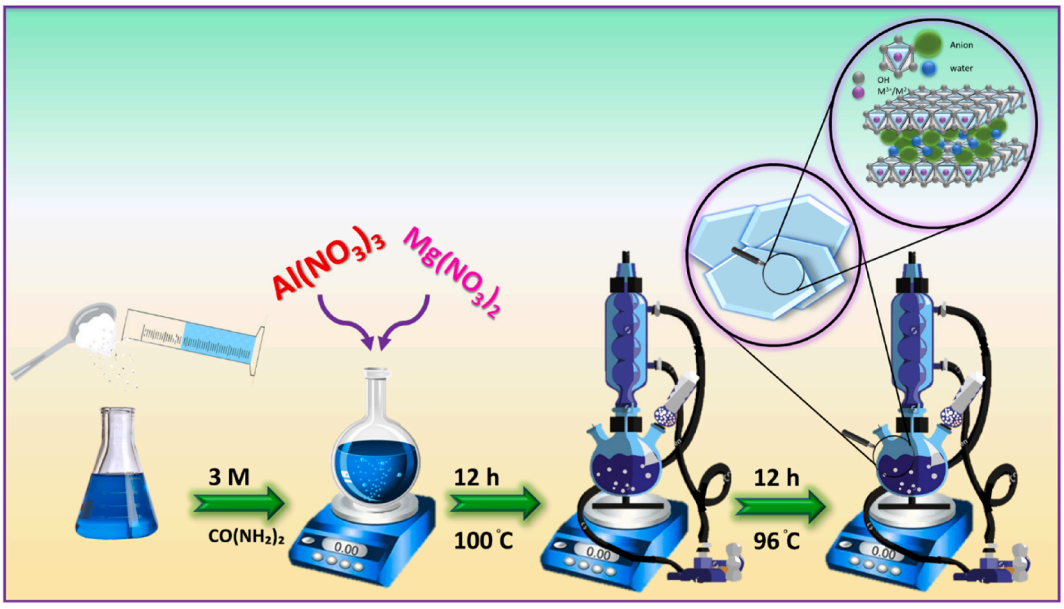

Scheme 2. General procedure for the preparation of Mg–Al-LDH.

2.4. Preparation of Mg–Al LDH-TMA nanocomposite

This point of the synthesis involved adding dichloromethane (CH_2Cl_2, 7 mL) solvent to the precipitate that was generated in the previous step. Next, synthesized LDH (0.5 g) was added to the above solution, and last, tri-ethylamine (TEA, 0.3 mL) was added dropwise. Triethylamine, a weak base, oxidizes and separates the hydrogen atoms of OHs that are bound to the surface of LDH. This allows the hydroxyl functional group to be converted into O^-, which then attacks the chlorinated trimesic acid compound to facilitate their attachment. After sealing the glass flask's intake, the mixture was constantly stirred for 24 h at room temperature. The resulting Mg–Al LDH–TMA composite was collected via centrifugation, washed with water, and dried at 80 °C for 24 h (Scheme 4).

3. Results and discussion

The FTIR spectra of the Al–Mg LDH is shown in Fig. 1a. The stretching vibrations of metal hydroxide octahedral complexes (M − O) bonds, where M can be either Mg^{2+} or Al^{3+}, have peaks in the range of 450–1124 cm^{-1}. The strong adsorption band between 1355 cm^{-1} and 1387 cm^{-1}, as depicted in the figure, relates to the stretching vibrations of the nitrate anions group [51]. The interlayer water molecule bending vibrations are attributed to the peaks at around 1542 cm^{-1} and 1621 cm^{-1}, the peak observed in the wave number of 2700–3716 cm^{-1} in LDH spectra were associated with the H–O bond's stretching vibrations [52]. The IR spectra of the Mg–Al LDH-TMA nanocomposite is displayed in Fig. 1b. The stretching vibrations of metal oxide (M − O) bonds are correlated with the peaks at the 490-900 cm^{-1} range. The aromatic ester's C–O stretching vibration is associated with a comparatively sharp peak in the 1222 cm^{-1} area (Given that trimesic acid has three carboxyl groups, several types of esters can be formed: Monoesters, diesters, triesters.). An average peak in the region of 1386 cm^{-1} corresponds with the carboxylic acid's O–H bond's bending vibration. The stretching vibration of the aromatic C═C bond relates to the peak in the 1560 cm^{-1} area. The two-branched strong peak at 1650 cm^{-1} and 1760 cm-1 attributed to the stretching vibrations of C═O of the acid and ester functional groups in the nanocomposite, respectively. Furthermore, the stretching vibration of the carboxylic acid's H–O bond is responsible for the bord peak observed at the 3700–2500 cm^{-1} area.

The XRD spectrum of Mg–Al LDH is presented in Fig. 2a. It reveals the presence of four main peaks related to the crystal structure of LDH, at 2θ of 11.735, 23.631, 35.003, 39.632, 47.228, 61.018 and 62.318 respectively, to the crystallographic planes (003), (006), (009), (015), (012), (110) and (113) of the crystalline phase of nanoparticles [53]. No additional peaks are observed, indicating the highly pure and crystalline LDH layers. The corresponding Mg–Al LDH is well matched with the JCPDS card number (00-014-0191), indicating the successful synthesis of Mg–Al LDH.

The peaks of the X-ray diffraction pattern associated with the manufactured Mg–Al LDH-TMA nanocomposite are depicted in Fig. 2b. This pattern not only validates the existence of LDH (JCPDS 00-014-0191), but also that trimesic acid (JCPDS 00-045-1880) is present in the nanoadsorbent. Also, the nanocomposite's XRD pattern clearly shows diffraction peaks associated with the structure of trimesic acid and LDH.

Thus, it can be said that during the creation of the Mg–Al LDH-TMA nanocomposite, the crystal structures of trimesic acid and LDH do not change.

The results of the EDS analysis of the synthesized nanocomposite is shown in Fig. 3. The peaks of C (33.41) and O (53.55) elements

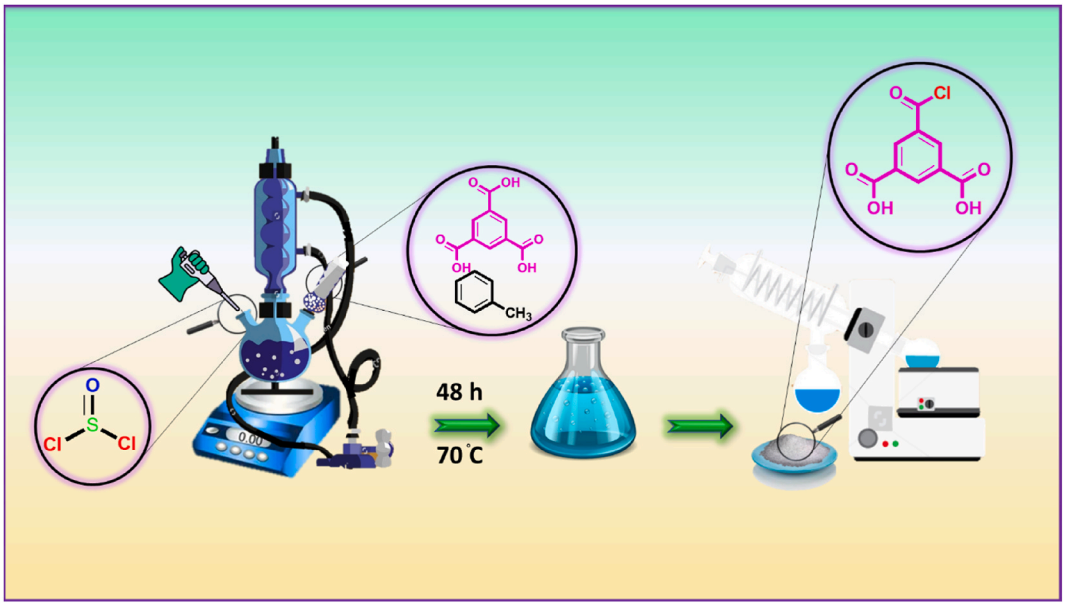

Scheme 3. General procedure for preparation method of TMA.

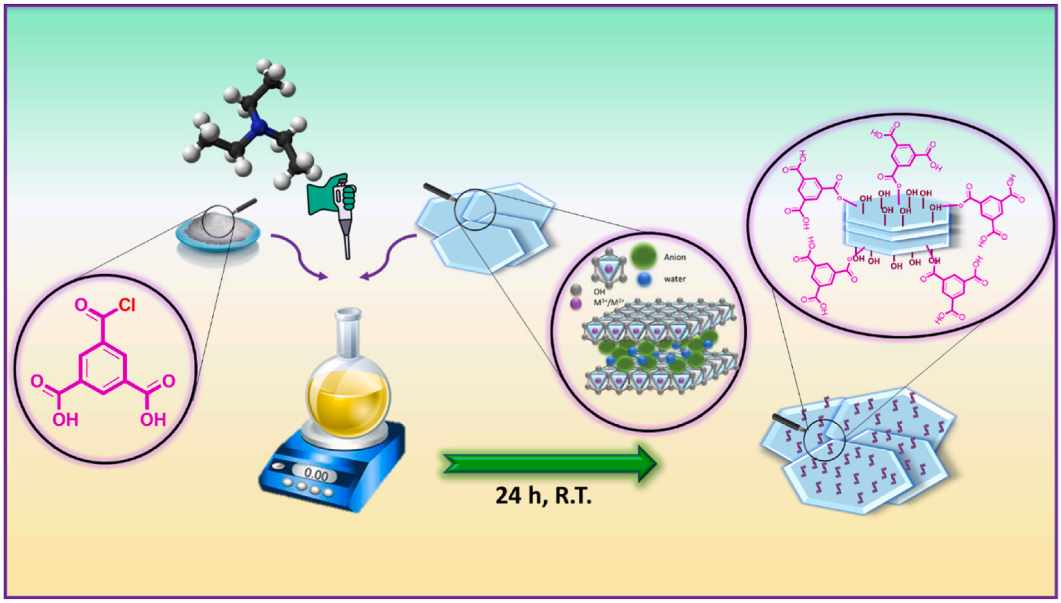

Scheme 4. General procedure for the preparation of LDH–TMA nanocomposite.

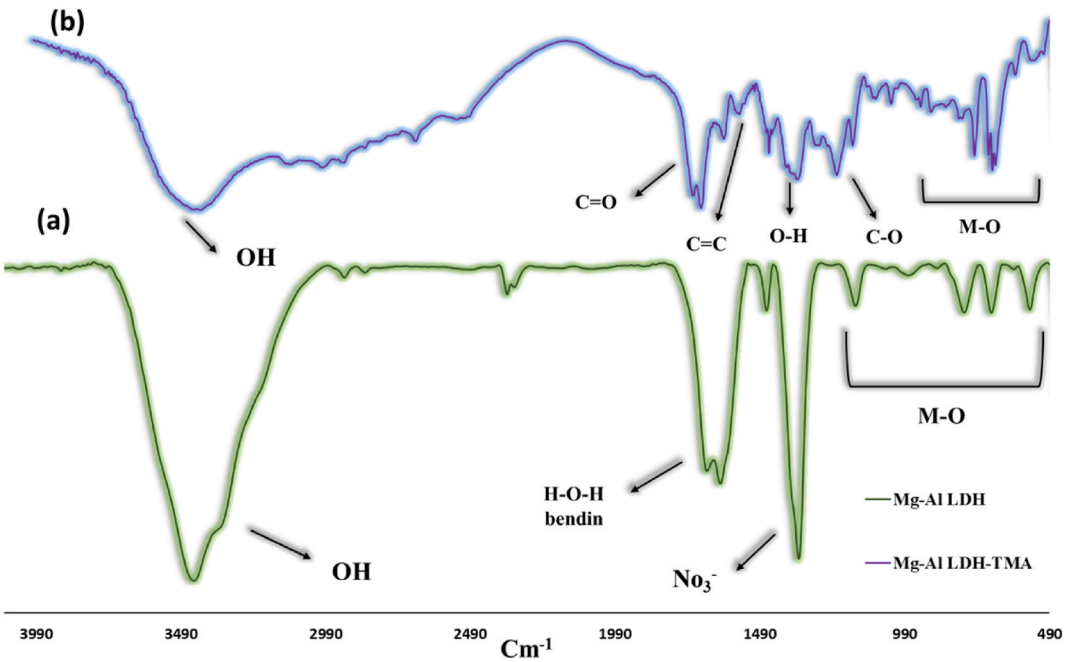

Fig. 1. FTIR spectra of Al–Mg LDH (a), and LDH–TMA nanocomposite (**1, b**).

confirm that trimesic acid is present in the nanocomposite structure; the peaks of Al (4.06) and Mg (4.58) can be attributed to the LDH portion of the nanocomposite; the peak of N (4.39) element is also related to interlayer nitrate ions.

The FE-SEM images of the synthesized Mg–Al LDH are displayed in Fig. 4 (a-d). Successful synthesis of LDH is indicated by the images, which clearly reveal hexagonal and assembled crystal plates with a thickness of around 20–100 nm. Additionally, in Fig. 4, parts (e-f) of the FE-SEM images in different magnifications pertaining to the synthesized nanocomposite are shown. The origins and composition of the globules on the surface of LDH platelets are associated with the organic component of the nanocomposite, TMA, which is linked to LDH through the ester bond formed between the carboxylic acid functional group of TMA and the hydroxides of the LDH surface. It is evident from these images that the TMA agent has uniformly functionalized the Mg–Al LDH base material, maintaining its layered structure and preventing lumps.

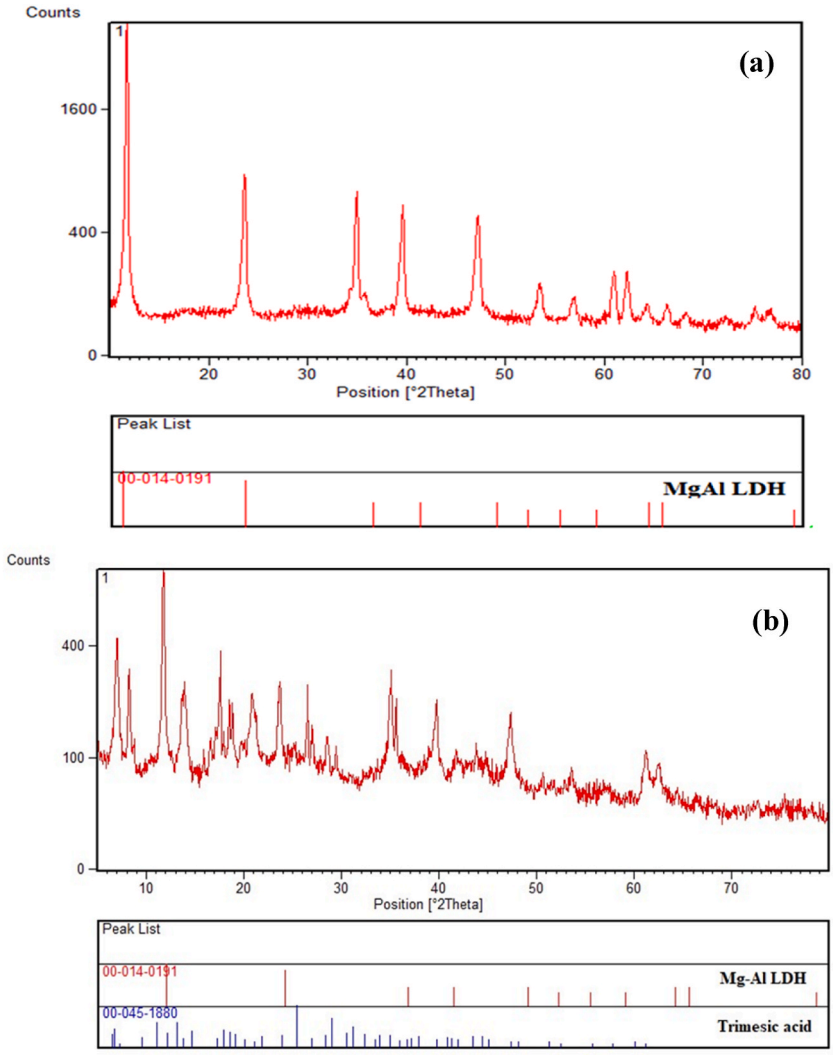

Fig. 2. XRD patterns of Al–Mg LDH (**a**), and LDH–TMA nanocomposite (**1, b**).

The synthesized Mg–Al LDH-TMA nanocomposite's TGA analysis curve is depicted in Fig. 5. At the range of 100–110 °C, a typical TGA baseline shows an apparent weight gain due to buoyancy. As the temperature increases, the gas surrounding the sample pan becomes less dense, so the pan experiences less buoyant lift (per Archimedes' principle). The temperature range of 130–230 °C is where the first observed weight loss (∽10 %) occurred, which is because of the evaporation of solvents and water molecules trapped between the layers. Around 230 to 480 °C (∽20 %) degrees is when trimesic acid, the organic components of the nanocomposite, breaks down. Since organic materials usually break down at 400°, trimesic acid's hydrogen bonding with the agent OH in LDH may be the cause of the organic components' remarkable temperature tolerance in this nanocomposite. Between 480 and 800 °C (∽31 %) is when the mineral component of the nanocomposite breaks down.

Poresize distribution measurements for Mg–Al LDH-TMA and N_2 adsorption/desorption isotherms were carried out in order to gain a better knowledge of the structural characteristics of adsorbents. As can be shown, the Mg–Al LDH-TMA nanocomposite had a pore volume of 0.04 cm^3/g and a low BET surface area of 17.21 m^2/g (Fig. 6 and Table 1). The composite may therefore offer more suitable binding sites during adsorption, improving the dyes' adsorption performance, as seen by the N_2 adsorption/desorption data. Additionally, the mesoporous structure of the Mg–Al LDH-TMA was revealed by the porediameter distribution. Furthermore, the 2D layered hydrotalcite's nanosheet shape helped to maximize contact with the TMA, enhancing the combination's adsorption efficacy.

4. Optimization of dye removal experiments using Mg–Al LDH–TMA nanocomposite (1)

The effect of adjusting a number of experimental parameters, such as contact time, adsorbent dosege, pH, and temperature, on the adsorption of MB and IC on Mg–Al LDH-TMA nanocomposite, provided a comprehensive understanding of the mechanism behind dye adsorption. The adsorbent was filtered out of the aqueous solution after varying periods of contact; the removal percentage (R%) is a

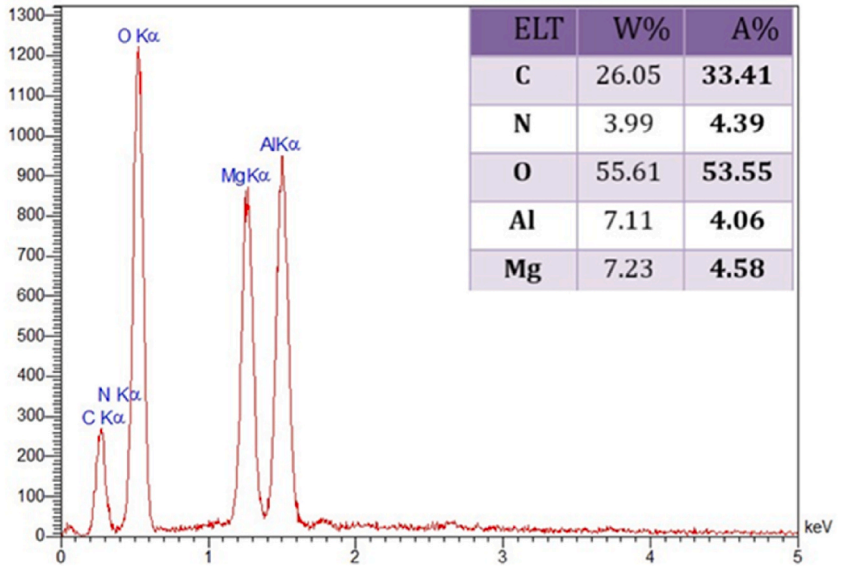

Fig. 3. EDX spectra of Mg–Al LDH–TMA nanocomposite (**1**).

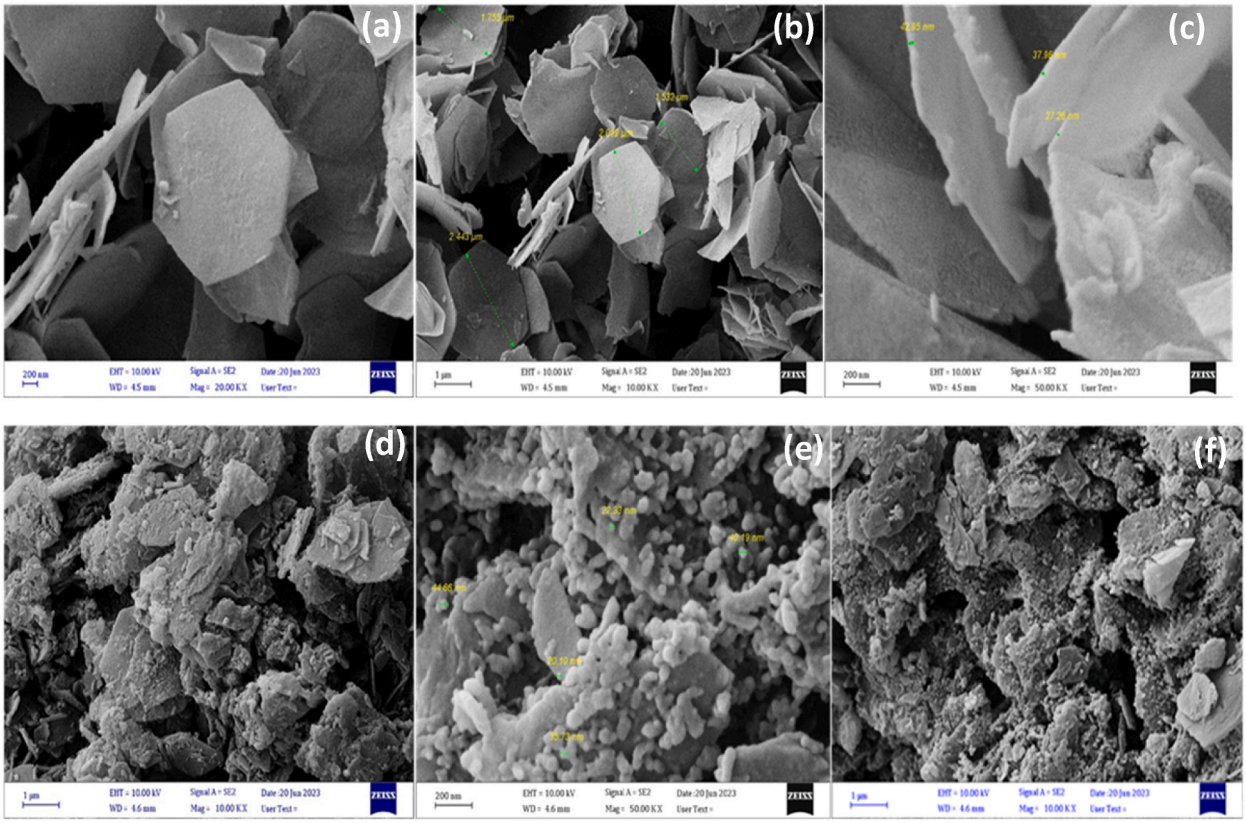

Fig. 4. FESEM images of Mg–Al LDH (**a**, **b** and **c**) and Mg–Al LDH–TMA nanocomposite (**d**, **e** and **f**).

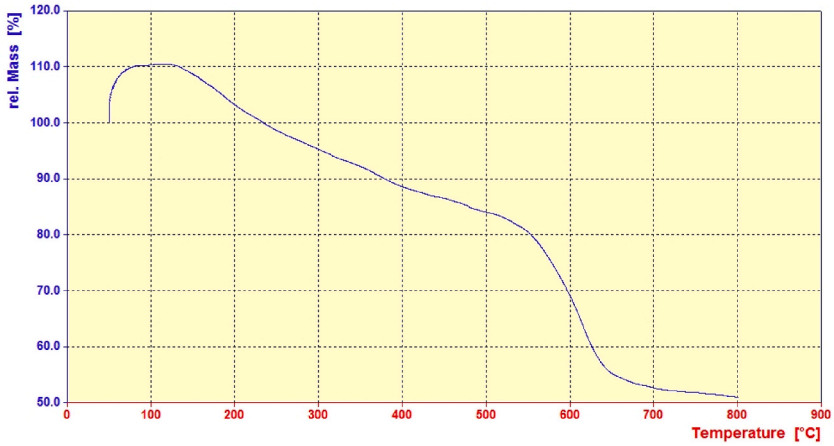

Fig. 5. TGA curve of the Mg–Al LDH–TMA nanocomposite (**1**).

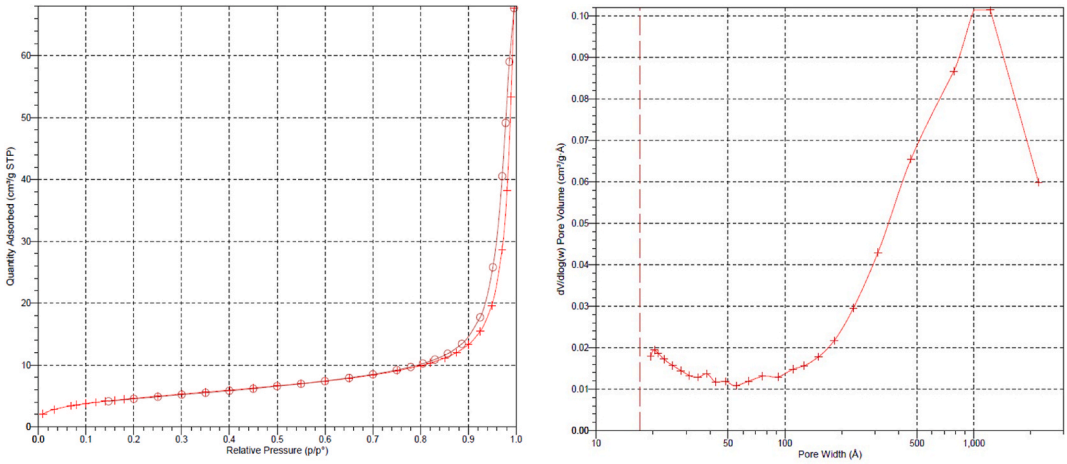

Fig. 6. N_2 adsorption–desorption isotherms of Mg–Al LDH–TMA nanocomposite (**1**).

Table 1
Structural parameters of Cu–Al LDH, and Mg–Al LDH-TMA nanocomposite determined from nitrogen sorption experiments.

Sample	S_{BET}[a]/$m^2\ g^{-1}$	V_p[b]/$cm^3\ g^{-1}$	D_p[c]/nm
Mg–Al LDH-TMA	17.21	0.04	10.295

[a] Specific surface area calculated by the BET method.
[b] Total pore volume registered at $P/P_0 = 0.20$.
[c] Pore size diameter calculated by the BJH method.

measure of how effectively the adsorption process has removed contaminants from the initial solution, and adsorption capacity (qt in mg/g) were computed using **Eqs. (1) and (2)**:

$$\text{Dye Removal } \% = \frac{C_{0-}\ C_e}{C_0} * 100 \tag{1}$$

$$q_{e=\frac{(C_{0-}\ C_e)V}{W}} \tag{2}$$

where W (mg) represents the mass of the sorbent, V (L) is the volume of the MB and IC dyes solution, Co (mg/L) is the MB and IC concentration at the beginning, and Ce (mg/L) is the equilibrium MB concentration.

4.1. Equilibrium studies

In order to study the MB and IC dye in equilibrium, 5 mg of sorbent were shaken with 100 mL solution containing different MB and IC concentrations (10–50 mg/L) at pH = 7 and 30 °C for 60 min. With the solutions filtered, a UV–Vis spectrophotometer was used to measure the adsorbance at 610 nm and 664 nm for IC and MB, respectively.

4.2. Effect of initial concentration of dyes

In order to examine the impact of concentration on adsorption, a magnet was used to mix solutions containing 10, 20, 30, 40, 50, 60, and 70 mg/L of methylene blue dye and 10, 20, 30, 40, and 50 mg/L of indigo carmine dye with 0.005 g of adsorbent for 60 min. Following the adsorption process, the solutions were then filtered to separate the adsorbent. The optimum adsorption capacities for methylene blue and indigo carmine are 40 mg/L and 60 mg/L, respectively, as shown in Fig. 7.

4.3. Adsorbent dose effect

In an effort to examine how the dosage of the adsorbent affects the ability of the Mg–Al LDH-TMA nanocomposite to adsorb the dyes indigo carmine and methylene blue, 1, 3, 5, 7, and 9 mg of the nanocomposite were used at room temperature and neutral pH, with the optimal concentrations of 40 mg/L for indigo carmine and 60 mg/L for methylene blue. The mixture was then stirred for 1 h using a magnetic stirrer. For indigo carmine dye, the optimum adsorbent dosage was 3 mg, whereas for methylene blue dye, the value was 1 mg. It is generally possible to conclude that increasing the adsorbent dose in both dyes has resulted in a decrease in adsorption capacity, as Fig. 8 illustrates. One of two possible explanations for this decrease is that, while dye concentration and volume remain constant, the competition for dye molecules increases as the concentration of Mg–Al LDH-TMA nano adsorbent particles rises. This may result in a decrease in the number of adsorption sites available to the special Mg–Al LDH-TMA nanoparticles, making it more challenging for them to adsorb dye molecules. Secondly, when the dose of the adsorbent is increased, the concentration of it's site causes adsorbents to overlap, which accumulates particles and blocks pores or active sites on the adsorbent's surface, lowering the adsorbent's equilibrium and capacity.

4.4. Contact time effect

Investigating the relationship between contact duration and adsorption capacity is one of the most important parts of the adsorption process research. Adsorption was tested in the intervals of 15, 30, 60, 90, and 120 min, and under optimal circumstances, the concentration of indigo carmine was 40 mg/L and the adsorbent dose was 0.003 g, while the concentration of methylene blue was 60 mg/L and the adsorbent dose was 0.001 g. This was carried out in order to examine how the time procedure affected the adsorption capacity of the dyes. Based on the information gathered from Fig. 9, it can be deduced that rapid adsorption and an increase in adsorbent capacity occurred with an increase in contact time, particularly in the early stages, because of the strong attraction between the adsorbent and the dye and the abundance of adsorption sites. Has been located as a result, 60 min was the ideal duration for indigo carmine dye and 90 min for methylene blue dye. When the process is carried out beyond the optimal times, the amount of dye adsorption remains nearly constant over time. This is because the adsorbent dye saturates the adsorption sites, slowing down the adsorption speed in the last stages of the adsorption process.

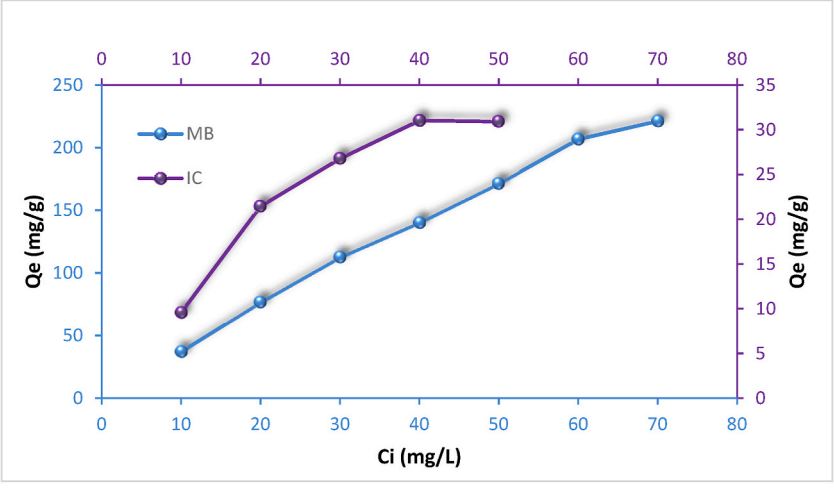

Fig. 7. Effect of the initial concentration for the adsorption of MB and IC (C_0 = 10–60 mg/L, pH = 7, T = 30 °C, m = 5 mg, t = 60 min).

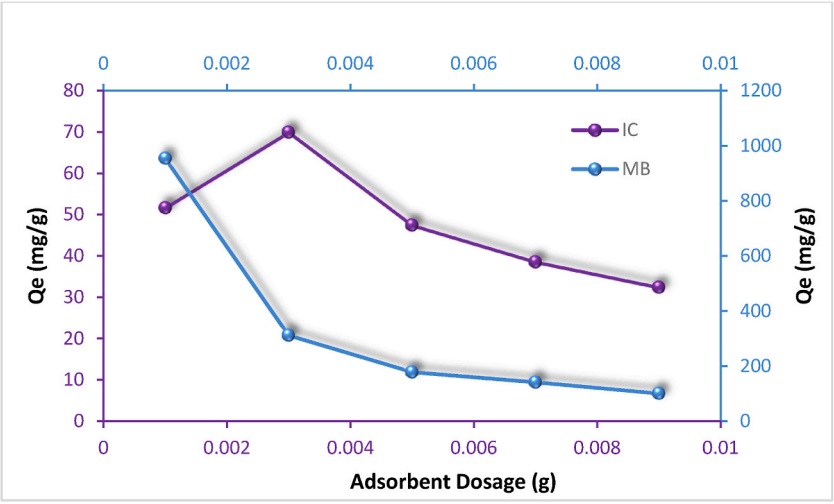

Fig. 8. Effect of the adsorbent dose for the adsorption of MB and IC (pH = 7, T = 30 °C, m = 1–9 mg, t = 60 min).

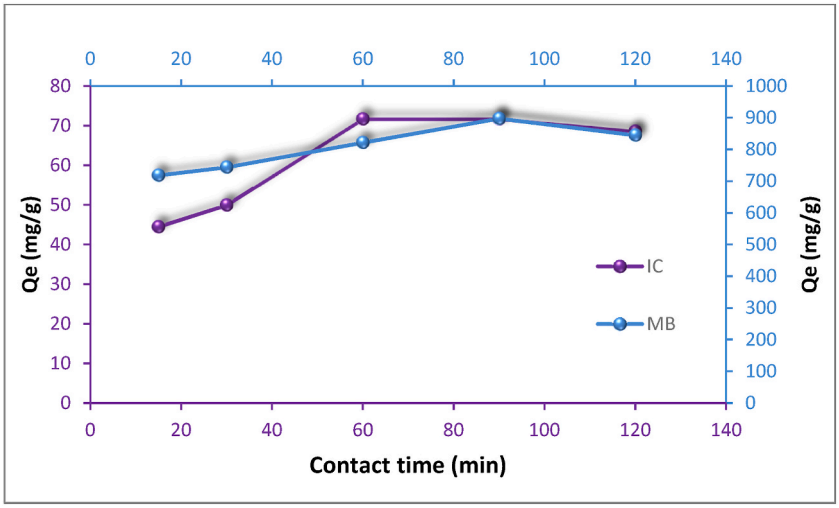

Fig. 9. Effect of the time on MB and IC adsorption.

4.5. *Effect of temperature*

One of the **key elements** that significantly affects surface adsorption is temperature. The type of surface material, the type of adsorber (molecule or particle), and the ambient factors all affect how temperature affects surface adsorption. Investigated and examined were the effects of temperature variations on adsorption at 25, 40, 60, 80, and 90 °C, as well as under ideal conditions for indigo carmine (40 mg/L, 0.003 g of adsorbent dose, and 60 min of adsorption time), and methylene blue (60 mL/L, 0.001 gr of adsorbent dose, and 90 min of adsorption time). The data presented in Fig. 10 reveals that the adsorption capacity of indigo carmine reduces as temperature increases from 60 to 90 °C, but it increases from 25 to 60 °C. This suggests that the adsorption process is performing exothermically. Furthermore, the temperature-dependent adsorption capability of methylene blue dye has been seen to diminish above 25 °C. There are several reasons for this drop in methylene blue dye adsorption in Mg–Al LDH-TMA nano-adsorbent with rising temperature, several of which relate to the adsorption process's thermodynamics. Is going to Many times, dyes like methylene blue adsorb on solid adsorbents in an exothermic process, which releases heat as the dye molecules attach to the Mg–Al LDH-TMA nano adsorbent's surface. In an attempt to maintain equilibrium as the temperature rises, the system lowers its adsorption capacity. Le Chatelier's principle, which says that an equilibrium system adapts to any change in its environment, explains this. Conversely, elevated temperatures have the potential to interfere with the adsorption forces that hold dye molecules to the Mg–Al LDH-TMA nano-adsorbent surface. Higher temperatures release thermal energy that causes the dye molecules to either diffuse or detach from the adsorbent surface, reducing their overall affinity for Mg–Al LDH-TMA. This results in a reduction of the adsorption capacity. At higher temperatures, the adsorption efficiency can be counteracted by other competing processes, such as dye desorption,

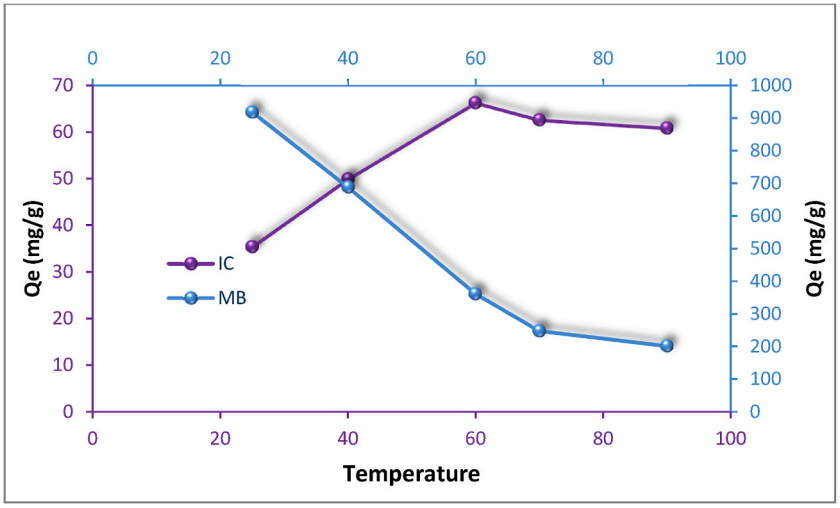

Fig. 10. Effect of temperature on MB and IC adsorption.

dye degradation, or modifications to the structure and stability of the Mg–Al LDH-TMA nano adsorbent.

4.6. Influence of solution pH on adsorption behaviour

The effect of pH changes on dye adsorption is depicted in Fig. 11. The reason for the variation in dye adsorption in the Mg–Al LDH-TMA nanocomposite with pH changes is that both the surface charge of the adsorbent material and the surface charge of the adsorbed material's molecules are impacted by pH. This pH-dependent behaviour is associated with electrostatic interactions between charged species involved in the adsorption process. Due to the protonation of hydroxyl groups ($OH^- \rightarrow OH_2$), the Mg–Al LDH-TMA nano sorbent typically exhibits a positive surface charge at low pH values (acidic circumstances). The molecules of indigo carmine, which are anionic at this pH, are drawn to the positively charged surface. When the pH is higher (alkaline circumstances), the hydroxyl groups ($OH^- \rightarrow O$) deprotonate, resulting in a negatively charged surface for the Mg–Al LDH-TMA nanocomposite, therefore negatively charged indigo carmine molecules are repelled by this negative surface charge. As anticipated, the adsorption capacity of MB rises as the pH of the solution decreases because the surface progressively becomes negatively charged. Consequently, the adsorption capacity can be enhanced through adsorbent negative charges increasing the electrostatic attraction.

5. Kinetics study

The dye's adsorption kinetics were examined in the presence of 0.001 g of nanocomposite at pH 11, 25 °C, and an initial concentration of 40 mg/L for methylene blue, and 0.003 g of nanocomposite at pH 7, 60 °C, and an initial concentration of 60 mg/L for indigo carmin. After stirring the mixture for 15, 30, 60, 90, and 120 min, samples were filtered to ensure there were no particles in it. **Eqs** (**3**) and (**4**) represent the pseudo-first-order and pseudo-second-order models that were used to test the kinetic data for MB and IC adsorption.

$$\log(qe - qt) = logqe - \left(\frac{K_1}{2.303}\right)t \tag{3}$$

$$\frac{t}{q_t} = \frac{1}{K^2 q_e{}^2} + \left(\frac{1}{q_e}\right)t \tag{4}$$

where the adsorption capacity and the adsorption capacity in time are denoted by q_e (mg/g) and q_t (mg/g), respectively, and the first- and second-order adsorption kinetics are represented by k_1 (1/min) and k_2 (g/mg. min). The correlation factor (R^2) of the pseudo-second-order model for the Mg–Al LDH–TMA nanocomposite was 1. These findings suggest that the pseudo-second-order kinetics model can adequately explain the MB and IC adsorption on the Mg–Al LDH–TMA nanocomposite. These various kinetic relationships are shown in Fig. 12 (a,b) and Table 2.

6. Adsorption isotherms

Further research into the adsorption of MB and IC on the Mg–Al LDH-TMA nanocomposite was conducted using the Langmuir **Eq.** (**5**) and Freundlich **Eq.** (**6**) isotherms [54,55].

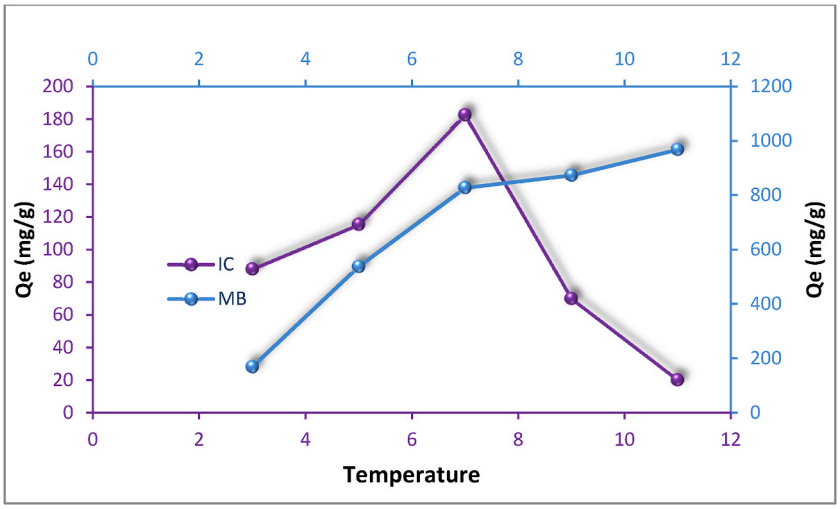

Fig. 11. Effect of pH on MB and IC adsorption.

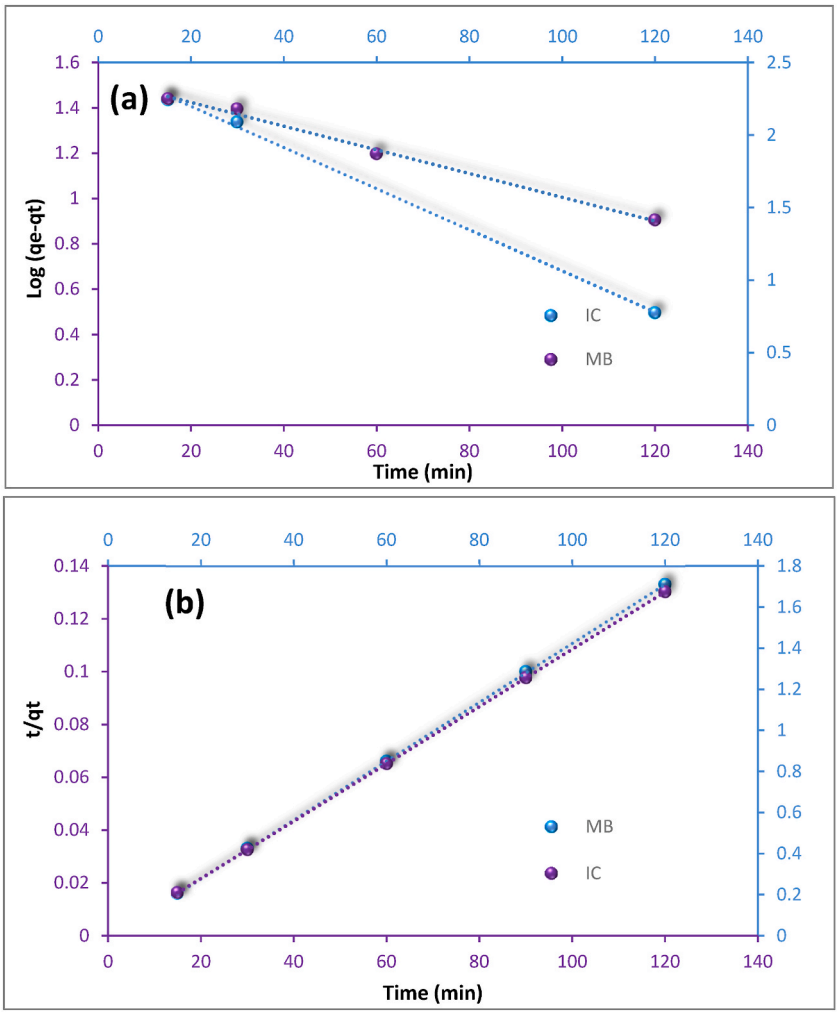

Fig. 12. Adsorption kinetics of MB and IC on LDH–TMA nanocomposite: (a) Pseudo-first-order, and (b) Pseudo-second-order models.

Table 2
Pseudo-first order and pseudo-second order kinetic parameters for MB and IC adsorption by LDH-TMA nanocomposite.

Models	Parameters	IC	MB
Pseudo-first-order	qe, calc (mg/g)	38.815	254.097
	K1	0.0209	0.2003
	R2	0.9986	0.9748
Pseudo-second-order	qe, calc (mg/g)	71.42	909.09
	K2	0.49	0.002
	R2	1	1

$$\frac{C_e}{q_e} = \frac{1}{K_L q_m} + \frac{1}{q_m} C_e \tag{5}$$

$$ln\ q_e = ln\ K_F + \left(\frac{1}{n}\right) ln\ C_e \tag{6}$$

where the values of qe (mg/g) and Ce (mg/L), respectively, denote the concentration of MB and IC and the adsorption capacity of the MB and IC adsorbed in equilibrium. Freundlich constants KF (mg/g) and n are used to describe the adsorption intensity and capacity, respectively; the equilibrium binding constant (L/mg) is represented by AT, and the Temkin constant is denoted by B. Fig. 13 (a, **b)**, Fig. 14 (a, **b)** and Fig. 15 (a, **b)** present a comparison of the experimental data for the MB and IC adsorption on the Mg–Al LDH–TMA nanocomposite with the linear diagram of the Langmuir, Freundlich, and Temkin isotherm models. The adsorption isotherm is more compatible with the Freundlich adsorption model, as indicated by the greater linear fit correlation coefficient (R^2) of the Freundlich

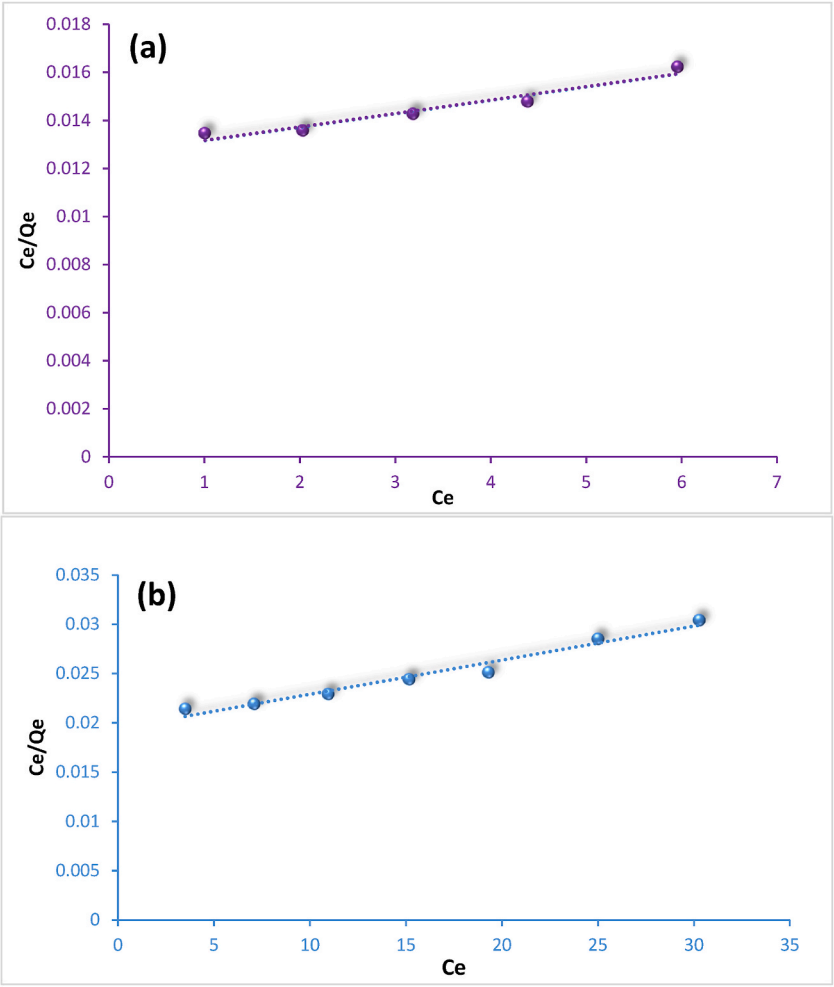

Fig. 13. Equilibrium studies of IC (**a**) and MB (**b**) adsorption using Mg–Al LDH–TMA nanocomposite, Langmuir isotherm model.

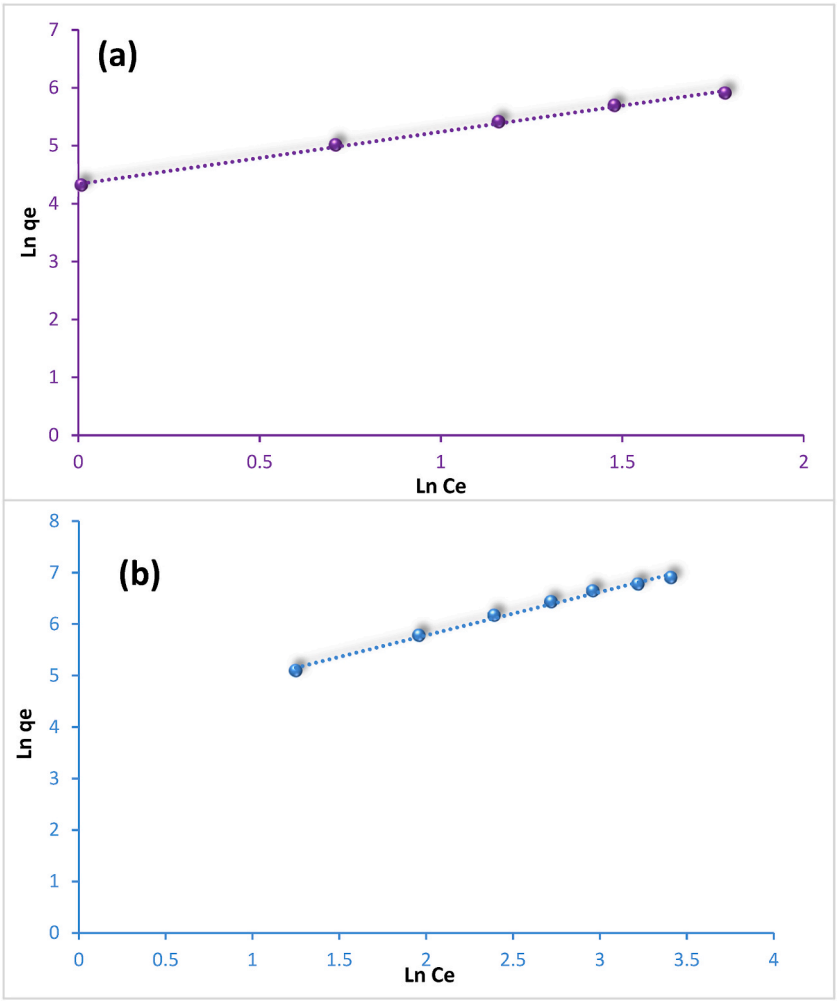

Fig. 14. Equilibrium studies of IC (**a**) and MB (**b**) adsorption using Mg–Al LDH–TMA nanocomposite Freundlich isotherm model.

adsorption model in comparison to the Langmuir model. Additionally, at 25 °C and 60 °C for MB and IC, respectively, the maximal adsorption capacity was 3333.33 mg/g and 1666.66 mg/g (Table 3).

7. Adsorption mechanism

Scheme 5 shows the adsorption mechanism that uses Mg–Al LDH-TMA nanocomposite to remove MB and IC dyes. The Mg–Al LDH-TMA nanocomposite's structure shows that it contains three functional groups: carboxylic acid, aromatic ring and hydroxyl. Therefore, the potential source of adsorption could be the presence of an aromatic ring in trimesic acid, which can interact through π-π stacking interactions with the aromatic regions of IC and MB dye molecules. Moreover, trimesic acid contains carboxylic acid groups (-COOH), which can participate in hydrogen bonding and electrostatic interactions with other molecules. These functional groups can form complexes with metal ions present in the LDH layers, influencing the surface chemistry and adsorption properties. When incorporated into the LDH structure, trimesic acid can modify the surface properties of the nanocomposite, such as polarity and hydrophobicity/hydrophilicity. These modifications can affect the adsorption affinity and selectivity of the nanocomposite towards different molecules. Molecules can also adsorb onto the external surface of LDH particles via physical interactions such as van der Waals forces , electrostatic attraction and hydrogen bonding. This surface adsorption contributes to the overall adsorption capacity of the nanocomposite. The electrostatic interaction and hydrogen bonding between electron-rich oxygen and positively charged regions of the indigo carmine dye molecules, such as protonated amino groups or any other positively charged functional groups. MB and IC dye molecules can combine with carboxylic acid groups to form surface complexes, in which the dye molecules bind or coordinate with the LDH surface through particular interactions or coordination bonds [56,57].

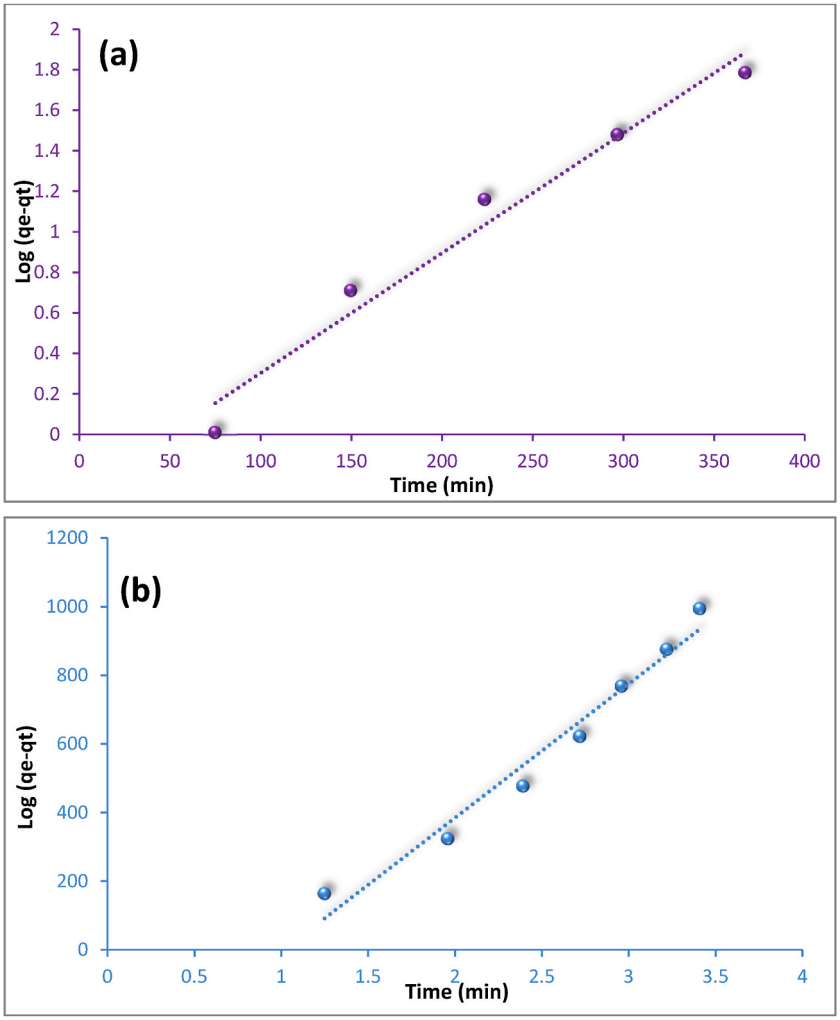

Fig. 15. Equilibrium studies of IC (**a**) and MB (**b**) adsorption using Mg–Al LDH–TMA nanocomposite, Temkin isotherm model.

Table 3
Langmuir and Freundlich isotherm parameters for MB and IC adsorption on Mg–Al LDH–TMA nanocomposite.

Models	Parameters	IC	MB
Langmuir	q_{max} (mg/g)	1666.66	3333.33
	K_L (L/mg)	0.047	0.0153
	R^2	0.9423	0.968
Freundlich	K_F (mg/g)	76.600	60.551
	n	1.107	1.189
	R^2	0.997	0.9929
Temkin	K_T	1.389	2.47
	B	163.79	395.59
	R^2	0.9691	0.9693

8. Recycling studies

The application of nanoadsorbents more especially, LDH nanocomposites has the potential to completely transform water treatment procedures. In order to improve their sustainability and environmental impact, this part analysis the recycling investigations carried out on the Mg–Al LDH-TMA nanocomposite. Adsorbent recycling is essential to sustainable water treatment since it ensures economic viability and reduces environmental impact. The reusability of Mg–Al LDH-TMA nanocomposites in eliminating MB evaluated by experiments with a cleaning agent mixture consisting of 0.1 mol/L of HCl and 0.1 mol/L of NaCl and for eliminating IC evaluated by experiments with a cleaning agent mixture consisting of 0.1 mol/L of NaOH and 0.1 mol/L of NaCl. To prepare it for

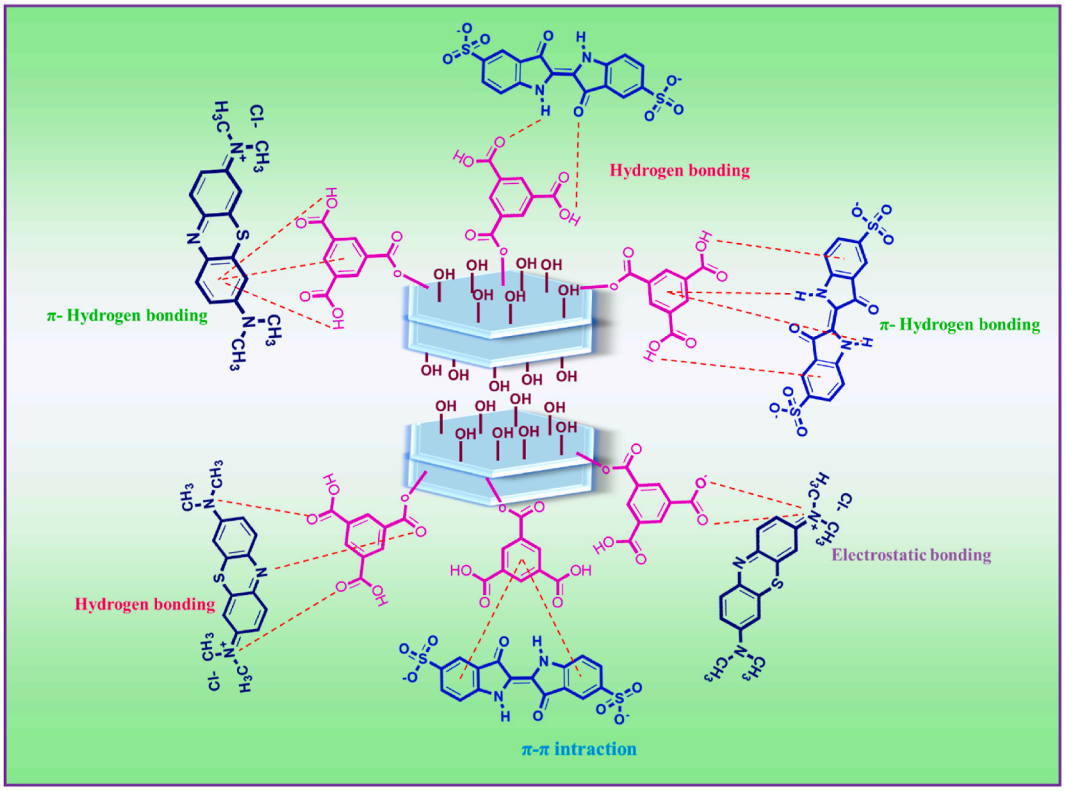

Scheme 5. The mechanism of MB and IC dye adsorption on the Mg–Al LDH-TMA nanocomposite.

further tests, the Mg–Al LDH-TMA nanocomposite was thoroughly washed after each application using a solution of 0.1 mol/L HCl for MB and 0.1 mol/L NaCl and 0.1 mol/L of NaOH and 0.1 mol/L of NaCl for IC. This was followed by 3 h of drying at 70 °C. To thoroughly verify the nanocomposites's reusability, this application, washing, and drying cycle was carried out four times, as shown in Fig. 16 and Fig. 17. Mg–Al LDH-TMA nanocomposites and other documented adsorbents are contrasted in Table 4 for their MB and IC adsorption capacities.

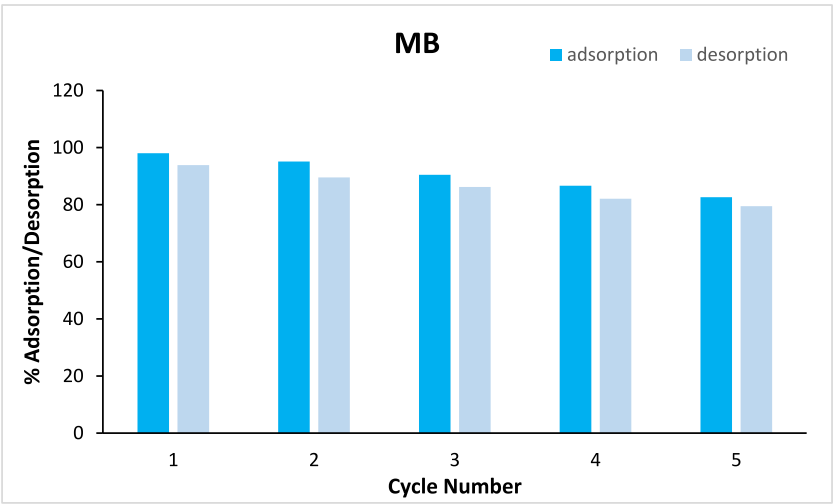

Fig. 16. Adsorption and desorption cycles of MB dye on Mg–Al LDH-TMA nanocomposite.

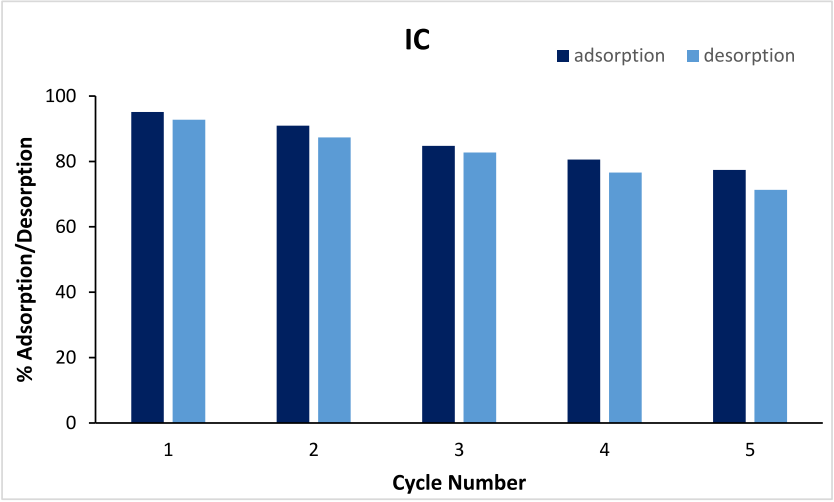

Fig. 17. Absorption and desorption cycles of IC dye on Mg–Al LDH-TMA nanocomposite.

Table 4
Compares the performance of the ability of the synthesized Mg–Al LDH-TMA nanocomposites in adsorbing MB and IC with other reported adsorbents.

Entry	Adsorbent	Adsorbent dose	Adsorption capacity (mg/g)	Dyre	Reference
1	CNT-TYR	0.01	434.08	MB	[58]
2	magnetic alginate/rice husk biocomposite	0.3	344	MB	[59]
3	BW(Ni)0.5	0.05	523.56	MB	[60]
4	Double cross-linked graphene aerogels	0.1	332.232	MB	[61]
5	Lathyrus sativus husk	5 mg/L	104.28	MB	[62]
6	LDH–polymer nanocomposite	0.001	1428.57	MB	[63]
7	CoZnAl-LDH/GO	0.02	169.49	MB	[64]
8	CuAl-LDH/SWCNTs	0.02	297.117	IC	[65]
9	CS/β-CD/STPP beads	500 mg/L	1000	IC	[66]
10	surfacemodified adsorbent prepared from municipal waste	0.05	146.3	IC	[67]
11	$MgFe_2O_4$	0.01	46.07	IC	[68]
12	Mg_2Al–Cl LDH	–	512.553	IC	[69]
13	Sn–MnO_2/CNT	0.005	714.28	IC	[70]
14	2.0 wt% Ag/UiO-66	0.05	312.6	IC	[71]
15	Mg–Al LDH-TMA	0.003	1666.66	IC	This work
16	Mg–Al LDH-TMA	0.001	3333.33	MB	This work

9. Conclusions

Mg–Al LDH-TMA nanocomposites stand out from other adsorbents due to their special qualities, which include their simple preparation process, high adsorption capacity, simplicity of removal, and reusable nature. The purpose of creating the Mg–Al LDH-TMA nanocomposite was to remove MB and IC from water. The Mg–Al LDH-TMA nanocomposite structure was successfully verified, as shown by spectroscopic investigation, which also revealed a strong attraction for MB and IC molecules. Moreover, kinetic analyses demonstrated that the MB and IC adsorption onto the Mg–Al LDH-TMA composite was accurately characterized by the pseudo-second-order model. The adsorption data for the Mg–Al LDH-TMA nanocomposite were confirmed to be adequate by the Freundlich isotherm model, which also showed multilayer adsorption behavior. It was discovered that the Mg–Al LDH-TMA nanocomposite had a maximum adsorption capacity of 3333.33 mg/g for MB and 1666.66 mg/g for IC, respectively.

Data availability

Statement Data will be made available on request.

CRediT authorship contribution statement

Hoda salamaat: Writing – review & editing, Writing – original draft, Project administration, Methodology, Formal analysis, Data curation. **Hossein Ghafuri:** Writing – review & editing, Writing – original draft, Formal analysis, Data curation. **Nastaran Ghanbari:** Writing – review & editing, Writing – original draft, Software, Project administration, Methodology, Formal analysis, Data curation.

Declaration of competing interest

The authors declare that they have no known competing financial interests or personal relationships that could have appeared to influence the work reported in this paper.

Acknowledgements

We are grateful for the financial support from The Research Council of Iran University of Science and Technology (IUST), Tehran, Iran.

Appendix A. Supplementary data

Supplementary data to this article can be found online at https://doi.org/10.1016/j.heliyon.2024.e33656.

References

[1] M. Ahmed, A. Mohamed, An efficient adsorption of indigo carmine dye from aqueous solution on mesoporous Mg/Fe layered double hydroxide nanoparticles prepared by controlled sol-gel route, Chemosphere 174 (2017) 280–288.
[2] F. Ahmadijokani, R. Mohammadkhani, S. Ahmadipouya, A. Shokrgozar, M. Rezakazemi, H. Molavi, T.M. Aminabhavi, M. Arjmand, Superior chemical stability of UiO-66 metal-organic frameworks (MOFs) for selective dye adsorption, Chem. Eng. J. 399 (2020) 125346.
[3] D. Jiang, M. Chen, H. Wang, G. Zeng, D. Huang, M. Cheng, Y. Liu, W. Xue, Z. Wang, The application of different typological and structural MOFs-based materials for the dyes adsorption, Coord. Chem. Rev. 380 (2019) 471–483.
[4] C. Li, W. Wang, X. Sun, H. Hou, C. Zheng, J. Zhang, F. Hou, D. Zhang, J. Du, Y. Yao, Ultra-durable and flexible fibrous mild quasi-solid-state Ag–Zn batteries with Na 2 SO 4 electrolyte additive, J. Mater. Chem. A 10 (2022) 24708–24716.
[5] Y. Yang, C. Zhang, D. Huang, G. Zeng, J. Huang, C. Lai, C. Zhou, W. Wang, H. Guo, W. Xue, Boron nitride quantum dots decorated ultrathin porous g-C3N4: intensified exciton dissociation and charge transfer for promoting visible-light-driven molecular oxygen activation, Appl. Catal. B Environ. 245 (2019) 87–99.
[6] B. Song, Z. Zeng, G. Zeng, J. Gong, R. Xiao, M. Chen, X. Tang, S. Ye, M. Shen, Effects of hydroxyl, carboxyl, and amino functionalized carbon nanotubes on the functional diversity of microbial community in riverine sediment, Chemosphere 262 (2021) 128053.
[7] I. Ghanmi, W. Sassi, P. Oulego, S. Collado, A. Ghorbal, M. Díaz, Optimization and comparison study of adsorption and photosorption processes of mesoporous nano-TiO2 during discoloration of Indigo Carmine dye, Microporous Mesoporous Mater. 342 (2022) 112138.
[8] E. Sharifpour, M. Ghaedi, F. Nasiri Azad, K. Dashtian, H. Hadadi, M. Purkait, Zinc oxide nanorod-loaded activated carbon for ultrasound-assisted adsorption of safranin O: Central composite design and genetic algorithm optimization, Appl. Organomet. Chem. 32 (2018) e4099.
[9] K. Dashtian, S. Porhemat, A.R. Rezvani, M. Ghaedi, M.M. Sabzehmeidani, Adsorption of semisoft pollutants onto Bi2S3/Ag2S-AC under the influence of ultrasonic waves as external filed, J. Ind. Eng. Chem. 60 (2018) 390–400.
[10] M. Mon, R. Bruno, J. Ferrando-Soria, D. Armentano, E. Pardo, Metal–organic framework technologies for water remediation: towards a sustainable ecosystem, J. Mater. Chem. A 6 (2018) 4912–4947.
[11] Y. Wang, Q. Chang, C. Xue, J. Yang, S. Hu, Chemical treatment of biomass wastes as carbon dot carriers for solar-driven water purification, J. Colloid Interface Sci. 621 (2022) 33–40.
[12] A. Javed, A. Mushtaq, A critical review of electrocoagulation and other electrochemical methods, Int. J. Chem. Biochem. Sci 23 (2023) 98–110.
[13] G. Yu, Y. Wang, H. Cao, H. Zhao, Y. Xie, Reactive oxygen species and catalytic active sites in heterogeneous catalytic ozonation for water purification, Environ. Sci. Technol. 54 (2020) 5931–5946.
[14] K.S. Varma, R.J. Tayade, K.J. Shah, P.A. Joshi, A.D. Shukla, V.G. Gandhi, Photocatalytic degradation of pharmaceutical and pesticide compounds (PPCs) using doped TiO2 nanomaterials: a review, Water-Energy Nexus 3 (2020) 46–61.
[15] J. Khan, A.U. Khan, Y. Khan, Y. Wei, Q.U. Khan, S.I. Al-Saeedi, Controlled synthesis of Cadmium doped CuBi2O4 nanorods with rapid and synergistic visible light photocatalytic performance, Chem. Eng. Sci. 293 (2024) 120025.
[16] M. Yu, J. Wang, L. Tang, C. Feng, H. Liu, H. Zhang, B. Peng, Z. Chen, Q. Xie, Intimate coupling of photocatalysis and biodegradation for wastewater treatment: mechanisms, recent advances and environmental applications, Water Res. 175 (2020) 115673.
[17] E. Abdel-Halim, S.S. Al-Deyab, Chemically modified cellulosic adsorbent for divalent cations removal from aqueous solutions, Carbohydr. Polym. 87 (2012) 1863–1868.
[18] M. Cheng, Y. Liu, D. Huang, C. Lai, G. Zeng, J. Huang, Z. Liu, C. Zhang, C. Zhou, L. Qin, Prussian blue analogue derived magnetic Cu-Fe oxide as a recyclable photo-Fenton catalyst for the efficient removal of sulfamethazine at near neutral pH values, Chem. Eng. J. 362 (2019) 865–876.
[19] X. Wen, Z. Zeng, C. Du, D. Huang, G. Zeng, R. Xiao, C. Lai, P. Xu, C. Zhang, J. Wan, Immobilized laccase on bentonite-derived mesoporous materials for removal of tetracycline, Chemosphere 222 (2019) 865–871.
[20] C. Zhang, W. Wang, A. Duan, G. Zeng, D. Huang, C. Lai, X. Tan, M. Cheng, R. Wang, C. Zhou, Adsorption behavior of engineered carbons and carbon nanomaterials for metal endocrine disruptors: experiments and theoretical calculation, Chemosphere 222 (2019) 184–194.
[21] M. El-Kammah, E. Elkhatib, S. Gouveia, C. Cameselle, E. Aboukila, Enhanced removal of Indigo Carmine dye from textile effluent using green cost-efficient nanomaterial: adsorption, kinetics, thermodynamics and mechanisms, Sustainable Chemistry and Pharmacy 29 (2022) 100753.
[22] H. Sadegh, G. Ali, Potential Applications of Nanomaterials in Wastewater Treatment, 2018, pp. 51–61. June.
[23] V.K. Gupta, R. Kumar, A. Nayak, T.A. Saleh, M. Barakat, Adsorptive removal of dyes from aqueous solution onto carbon nanotubes: a review, Adv. Colloid Interface Sci. 193 (2013) 24–34.
[24] Y. Yao, F. Xu, M. Chen, Z. Xu, Z. Zhu, Adsorption behavior of methylene blue on carbon nanotubes, Bioresour. Technol. 101 (2010) 3040–3046.
[25] S. Wang, H. Sun, H.-M. Ang, M.O. Tadé, Adsorptive remediation of environmental pollutants using novel graphene-based nanomaterials, Chem. Eng. J. 226 (2013) 336–347.
[26] F. Ayari, G. Manai, S. Khelifi, M. Trabelsi-Ayadi, Treatment of anionic dye aqueous solution using Ti, HDTMA and Al/Fe pillared bentonite. Essay to regenerate the adsorbent, J. Saudi Chem. Soc. 23 (2019) 294–306.
[27] M.A.M. Salleh, D.K. Mahmoud, W.A.W.A. Karim, A. Idris, Cationic and anionic dye adsorption by agricultural solid wastes: a comprehensive review, Desalination 280 (2011) 1–13.
[28] C. Namasivayam, D. Kavitha, Removal of Congo Red from water by adsorption onto activated carbon prepared from coir pith, an agricultural solid waste, Dyes Pigments 54 (2002) 47–58.
[29] S. Tahir, N. Rauf, Removal of a cationic dye from aqueous solutions by adsorption onto bentonite clay, Chemosphere 63 (2006) 1842–1848.
[30] S. Sohrabnezhad, A. Pourahmad, Comparison absorption of new methylene blue dye in zeolite and nanocrystal zeolite, Desalination 256 (2010) 84–89.

[31] G. Crini, Kinetic and equilibrium studies on the removal of cationic dyes from aqueous solution by adsorption onto a cyclodextrin polymer, Dyes Pigments 77 (2008) 415–426.
[32] A.G. Prado, J.D. Torres, E.A. Faria, S.l.C. Dias, Comparative adsorption studies of indigo carmine dye on chitin and chitosan, J. Colloid Interface Sci. 277 (2004) 43–47.
[33] R. Moeinzadeh, N. Azizi, M. Hekmati, M. Qomi, D. Esmaeili, ZnONPs/covalent triazine frameworks nanocomposite as high-performance photocatalysts for degradation of Congo red under visible light, Mater. Chem. Phys. 307 (2023) 128122.
[34] Q. Fan, Z. Li, M. Li, X. Zhou, G. Zhang, S. Shen, In-situ generation of anti-fouling TpPa/PVDF membranes showing excellent photocatalytic degradation and self-cleaning for dyes in water, Separ. Purif. Technol. 343 (2024) 127167.
[35] V. Gadore, A.K. Singh, S.R. Mishra, M. Ahmaruzzaman, RSM approach for process optimization of the photodegradation of Congo red by a novel NiCo2S4/chitosan photocatalyst, Sci. Rep. 14 (2024) 1–20.
[36] M. Shabil Sha, H. Anwar, F.N. Musthafa, H. Al-Lohedan, S. Alfarwati, J.R. Rajabathar, J. Khalid Alahmad, J.-J. Cabibihan, M. Karnan, K. Kumar Sadasivuni, Photocatalytic degradation of organic dyes using reduced graphene oxide (rGO), Sci. Rep. 14 (2024) 3608.
[37] Y. Cao, D. Zheng, F. Zhang, J. Pan, C. Lin, Layered double hydroxide (LDH) for multi-functionalized corrosion protection of metals: a review, J. Mater. Sci. Technol. 102 (2022) 232–263.
[38] M. Ara, H. Ghafuri, N. Ghanbari, Copper (II) anchored on layered double hydroxide functionalized guanidine as a heterogeneous catalyst for the synthesis of tetrazole derivatives, Colloid and Interface Science Communications 53 (2023) 100704.
[39] L. Wang, Y. Wang, W. Lv, Y. Yao, Activation of peroxymonosulfate by MgCoAl layered double hydroxide: potential enhancement effects of catalyst morphology and coexisting anions, Chemosphere 286 (2022) 131640.
[40] G. Huang, C. Zhang, Z. Liu, S. Yuan, G. Yang, N. Li, Ultra-small NiFe-layered double hydroxide nanoparticles confined in ordered mesoporous carbon as efficient electrocatalyst for oxygen evolution reaction, Appl. Surf. Sci. 565 (2021) 150533.
[41] Y. Cao, S. Jin, D. Zheng, C. Lin, Facile fabrication of ZnAl layered double hydroxide film co-intercalated with vanadates and laurates by one-step post modification, Colloid and Interface Science Communications 40 (2021) 100351.
[42] H. Jabkhiro, K. El Hassani, M. Chems, A. Anouar, Simultaneous removal of anionic dyes onto Mg (Al) O mixed metal oxides from ternary aqueous mixture: Derivative spectrophotometry and Density Functional Theory study, Colloid and Interface Science Communications 45 (2021) 100549.
[43] J. König, Food Colour Additives of Synthetic Origin, Colour Additives for Foods and Beverages, Elsevier, 2015, pp. 35–60.
[44] E.P.o.F. Additives, N.S.a.t. Food, Scientific Opinion on the re-evaluation of Indigo Carmine (E 132) as a food additive, EFSA J. 12 (2014) 3768.
[45] M. Stolte, M. Vieth, Pathologic basis of mucosal changes in the esophagus. What the Endoscopist can (and must) see, Acta Endosc. 31 (2001) 125–129.
[46] M. El-Kammah, E. Elkhatib, S. Gouveia, C. Cameselle, E. Aboukila, Cost-effective ecofriendly nanoparticles for rapid and efficient indigo carmine dye removal from wastewater: adsorption equilibrium, kinetics and mechanism, Environ. Technol. Innovat. 28 (2022) 102595.
[47] C. Arora, S. Soni, S. Sahu, J. Mittal, P. Kumar, P. Bajpai, Iron based metal organic framework for efficient removal of methylene blue dye from industrial waste, J. Mol. Liq. 284 (2019) 343–352.
[48] M. Hu, H. Lou, X. Yan, X. Hu, R. Feng, M. Zhou, In-situ fabrication of ZIF-8 decorated layered double oxides for adsorption and photocatalytic degradation of methylene blue, Microporous Mesoporous Mater. 271 (2018) 68–72.
[49] I. Jack Clifton, J.B. Leikin, Methylene blue, Am. J. Therapeut. 10 (2003) 289–291.
[50] A.S. Alzaydien, Adsorption of methylene blue from aqueous solution onto a low-cost natural Jordanian Tripoli, Am. J. Appl. Sci. 6 (2009) 1047.
[51] S. Kundu, M.K. Naskar, Al–Mg–Ca-layered double oxides for efficient removal of as (v) from water: the role of amides, J. Chem. Eng. Data 64 (2019) 1594–1604.
[52] J.T. Kloprogge, L. Hickey, R.L. Frost, FT-Raman and FT-IR spectroscopic study of synthetic Mg/Zn/Al-hydrotalcites, J. Raman Spectrosc. 35 (2004) 967–974.
[53] X. Wang, X. Zhu, X. Meng, Preparation of a Mg/Al/Fe layered supramolecular compound and application for removal of Cr (VI) from laboratory wastewater, RSC Adv. 7 (2017) 34984–34993.
[54] Y. Li, J. Sun, Q. Du, L. Zhang, X. Yang, S. Wu, Y. Xia, Z. Wang, L. Xia, A. Cao, Mechanical and dye adsorption properties of graphene oxide/chitosan composite fibers prepared by wet spinning, Carbohydr. Polym. 102 (2014) 755–761.
[55] S.A. Elsayed, E.M. Saad, I.S. Butler, S.I. Mostafa, 2-Hydroxynaphthaldehyde chitosan schiff-base; new complexes, biosorbent to remove cadmium (II) ions from aqueous media and aquatic ecotoxicity against green alga Pseudokirchneriella subcapitata, J. Environ. Chem. Eng. 6 (2018) 3451–3468.
[56] T.J. Fraga, M.N. Carvalho, M.G. Ghislandi, M.A.d. Motta, Functionalized graphene-based materials as innovative adsorbents of organic pollutants: a concise overview, Braz. J. Chem. Eng. 36 (2019) 1–31.
[57] A.M. Aldawsari, I. Alsohaimi, H.M. Hassan, Z.E. Abdalla, I. Hassan, M.R. Berber, Tailoring an efficient nanocomposite of activated carbon-layered double hydroxide for elimination of water-soluble dyes, J. Alloys Compd. 857 (2021) 157551.
[58] M. Saxena, N. Sharma, R. Saxena, Highly efficient and rapid removal of a toxic dye: adsorption kinetics, isotherm, and mechanism studies on functionalized multiwalled carbon nanotubes, Surface. Interfac. 21 (2020) 100639.
[59] E. Alver, A.Ü. Metin, F. Brouers, Methylene blue adsorption on magnetic alginate/rice husk bio-composite, Int. J. Biol. Macromol. 154 (2020) 104–113.
[60] X. Yao, L. Ji, J. Guo, S. Ge, W. Lu, L. Cai, Y. Wang, W. Song, H. Zhang, Magnetic activated biochar nanocomposites derived from wakame and its application in methylene blue adsorption, Bioresour. Technol. 302 (2020) 122842.
[61] L. Jiang, Y. Wen, Z. Zhu, X. Liu, W. Shao, A Double cross-linked strategy to construct graphene aerogels with highly efficient methylene blue adsorption performance, Chemosphere 265 (2021) 129169.
[62] I. Ghosh, S. Kar, T. Chatterjee, N. Bar, S.K. Das, Removal of methylene blue from aqueous solution using Lathyrus sativus husk: adsorption study, MPR and ANN modelling, Process Saf. Environ. Protect. 149 (2021) 345–361.
[63] N. Ghanbari, H. Ghafuri, Design and preparation the novel polymeric layered double hydroxide nanocomposite (LDH/Polymer) as an efficient and recyclable adsorbent for the removal of methylene blue dye from water, Environ. Technol. Innovat. 26 (2022) 102377.
[64] M. Sharifi-Bonab, S. Aber, D. Salari, F. Khodam, Synthesis of CoZnAl-layered double hydroxide/graphene oxide nanocomposite for the removal of methylene blue: kinetic, thermodynamic, and isotherm studies, Environ. Prog. Sustain. Energy 39 (2020) e13316.
[65] N. Almoisheer, F.A. Alseroury, R. Kumar, M. Aslam, M. Barakat, Adsorption and anion exchange insight of indigo carmine onto CuAl-LDH/SWCNTs nanocomposite: kinetic, thermodynamic and isotherm analysis, RSC Adv. 9 (2019) 560–568.
[66] T. Kekes, C. Tzia, Adsorption of indigo carmine on functional chitosan and β-cyclodextrin/chitosan beads: equilibrium, kinetics and mechanism studies, J. Environ. Manag. 262 (2020) 110372.
[67] M.B. Ahmad, U. Soomro, M. Muqeet, Z. Ahmed, Adsorption of Indigo Carmine dye onto the surface-modified adsorbent prepared from municipal waste and simulation using deep neural network, J. Hazard Mater. 408 (2021) 124433.
[68] M. Adel, M.A. Ahmed, A.A. Mohamed, Effective removal of indigo carmine dye from wastewaters by adsorption onto mesoporous magnesium ferrite nanoparticles, Environ. Nanotechnol. Monit. Manag. 16 (2021) 100550.
[69] N. Li, Z. Chang, H. Dang, Y. Zhan, J. Lou, S. Wang, S. Attique, W. Li, H. Zhou, C. Sun, Deep eutectic solvents assisted synthesis of MgAl layered double hydroxide with enhanced adsorption toward anionic dyes, Colloids Surf. A Physicochem. Eng. Asp. 591 (2020) 124507.
[70] P. Saharan, A.K. Sharma, V. Kumar, I. Kaushal, Multifunctional CNT supported metal doped MnO2 composite for adsorptive removal of anionic dye and thiourea sensing, Mater. Chem. Phys. 221 (2019) 239–249.
[71] R.S. Salama, E.-S.M. El-Sayed, S.M. El-Bahy, F.S. Awad, Silver nanoparticles supported on UiO-66 (Zr): as an efficient and recyclable heterogeneous catalyst and efficient adsorbent for removal of Indigo Carmine, Colloids Surf. A Physicochem. Eng. Asp. 626 (2021) 127089.